Journal of Neuroscience Methods 224 (2014) 58–65

Contents lists available at ScienceDirect

Journal of Neuroscience Methods

journal homepage: www.elsevier.com/locate/jneumeth

Computational Neuroscience

Spectral factorization-based current source density analysis of ongoing neural oscillations

Ganesh B. Chand[a,*], Mukesh Dhamala[a,b]

[a] Department of Physics and Astronomy, Georgia State University, Atlanta, GA 30303, USA
[b] Neuroscience Institute, Georgia State University, Atlanta, GA 30303, USA

HIGHLIGHTS

- The proposed current source density (CSD) analysis applies to ongoing oscillations.
- This method does not require choosing a recording as a reference for the analysis.
- This method is validated in simulations and applied to local field potentials.
- This application produces meaningful results consistent with the earlier findings.

ARTICLE INFO

Article history:
Received 2 November 2013
Received in revised form
19 December 2013
Accepted 22 December 2013

Keywords:
Spontaneous neural oscillations
Neural current sources
Local field potentials
Evoked brain activity
Induced brain activity
Electrophysiological recordings

ABSTRACT

Background: Current source density (CSD) analysis is widely used in neurophysiological investigations intended to reveal the patterns of localized neuronal activity in terms of current sources and sinks. CSD is based on the second spatial derivatives of multi-electrode electrophysiological recordings, and can be applied to brain activity related to repeated external stimulations (evoked brain activity) or ongoing (spontaneous) brain activity. In evoked brain activity, event-related time-series averages of ensembles are used to compute CSD patterns. However, for ongoing neural activity, the lack of external events requires a different approach other than ensemble averaging.
New method: Here, we propose a new spectral factorization-based current source density (SF-CSD) analysis method for ongoing neural oscillations.
Results: We validated this new SF-CSD analysis method using simulated data and demonstrated its effectiveness by applying to experimental intra-cortical local field potentials recorded on multi-contact depth electrodes from monkeys performing selective visual attention tasks.
Comparison with existing methods: The proposed method gives space-unbiased estimates since it does not rely on a reference for CSD calculation in the frequency-domain.
Conclusion: The proposed SF-CSD method is expected to be a useful tool for systematic analysis of neural sources and oscillations from multi-site electrophysiological recordings.

1. Introduction

Neuronal cellular processes in the brain generate spatially distributed electric currents in the extracellular medium, giving rise to volume-conducted electric potentials throughout the brain (Buzsaki et al., 2012). The recordings of extracellular field potentials that index activity relevant to the local field potentials (LFPs), electroencephalography (EEG), and magnetoencephalography (MEG) do not necessarily represent spatially localized neuronal events because of reference dependence and inevitable volume-conducted field (Kajikawa and Schroeder, 2011). The underlying neuronal activity patterns are usually masked by these effects in multi-electrode potential recordings (Kajikawa and Schroeder, 2011). Current source density (CSD), expressed in terms of second spatial derivative (Laplacian transformation) of field potentials, minimizes non-local contributions such as reference-dependent and volume-conducted far-field effects from the field potentials. Therefore, CSD reveals more localized neuronal patterns (i.e., transmembrane currents in terms of sources and sinks) than the patterns of field potentials. The CSD analysis has been applied primarily to stimulus or task-evoked neural responses (Mitzdorf, 1985; Nicholson and Freeman, 1975), where the stimulus-triggered average responses are used to compute the CSD profiles. This technique is widely used

* Corresponding author. Tel.: +1 4044136073.
E-mail addresses: GCHAND1@STUDENT.GSU.EDU, GANESHCHAND64@GMAIL.COM (G.B. Chand).

0165-0270/$ – see front matter © 2013 Elsevier B.V. All rights reserved.
http://dx.doi.org/10.1016/j.jneumeth.2013.12.011

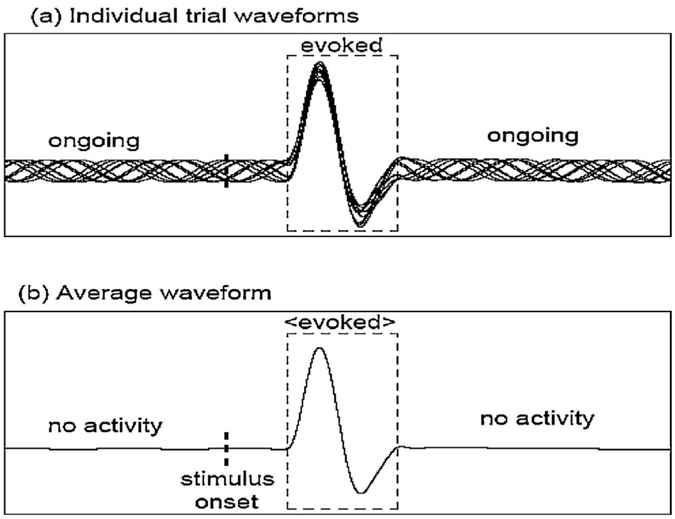

Fig. 1. The simulated waveforms of evoked brain responses and their averaged waveform. (a) Superimposed responses with ongoing and evoked activity, and (b) the waveform from ensemble averaging: ongoing activity is completely suppressed and only stimulus phase-locked evoked activity is retained.

especially in the layered structures of the brain, such as the cerebral cortex, hippocampus, or cerebellum (Bazhenov et al., 2011; Mehta et al., 2000a,b; Mitzdorf, 1985; Nicholson and Freeman, 1975).

Even in the absence of an external sensory stimulation or explicit task, the brain exhibits spontaneous activity (ongoing neural activity) reflecting the brain's self-organizing dynamic nature (Buzsaki, 2006). Such ongoing neural activity is captured both in intra-cranial and extra-cranial electrical recordings of a mammalian brain as oscillations in a broad range of frequencies from approximately 0.05–500 Hz (Buzsaki and Draguhn, 2004). These oscillations, which emerge within the brain as a consequence of neuronal firing and flow of synaptic inputs to neurons in a network, represent the brain's internal context for incoming sensory inputs (Fiser et al., 2004; Kenet et al., 2003; Tsodyks et al., 1999). A sensory input or a cognitive act is a tiny perturbation to these self-sustained and self-organized oscillations. A sensory evoked neural activity represents a minor departure of internally controlled robust ongoing network dynamics. When the stimulus presentation hits the brain at the peak of an ongoing oscillation, the stimulus-driven activity is amplified (Arieli et al., 1996; Dehaene et al., 2003). The stimulus-independent ongoing oscillations thus cannot be regarded as noise as in most of the studies of stimulus-evoked neural responses. The ongoing oscillations, which are phase-unlocked from trial to trial, can be suppressed by ensemble averaging as in stimulus-triggered averages of trials as shown by hypothetical waveforms in Fig. 1.

A different technique, other than ensemble averaging, is needed to preserve the overall ongoing neural activity (Csicsvari et al., 2003). The lack of an external trigger makes ensemble averaging difficult to achieve for ongoing neural activity. The studies of ongoing brain activity (Csicsvari et al., 2003; Lakatos et al., 2005) are relied on time-domain approach, where the waveform is detected by the peak activity. Meanwhile, single-trial CSDs are too noisy to be a reliable indicator of meaningful neural events. The phase realigned averaging technique (PRAT) (Chen et al., 2008; Dhamala et al., 2006) has tried to address this issue. However, the PRAT-based CSD uses a recording channel as a reference for realignment of trials and thus may often introduce a channel-specific bias in CSD estimates. Therefore, a systematic technique to compute the CSD profiles from trials of ongoing field potentials such as LFPs still remains a challenge. In the present work, we seek to develop a novel algorithm, named spectral factorization-based CSD (SF-CSD), to address this problem. To demonstrate applicability of the SF-CSD, we first apply it to simulated LFPs and then to the LFP recordings from a macaque monkey performing an intermodal selective attention task. By applying to simulated data, we check whether the proposed technique recovers the constructed architecture of the sources and sinks. By applying to the real electrophysiological data, we compare the results with those from the accepted methods.

The paper includes the following additional sections: materials and methods, results, and discussion. Section 2 encompasses the theoretical framework for SF-CSD analysis, details of parameters used in the LFPs simulation and in the LFP electrophysiological recordings. In the results section, we illustrate the workings of the SF-CSD algorithm on the LFPs simulated data and the LFPs recorded data from a monkey. Finally, we provide further discussion on the CSD analysis and overall usefulness of the SF-CSD algorithm.

2. Materials and methods

The time-domain CSD can be transformed into the frequency domain by using Fourier or wavelet spectral transformation. Equivalently, the frequency-domain CSD estimates from potential recordings are related to the second space derivative of Fourier (or wavelet) transforms of potential recordings, which is the basis of the proposed SF-CSD analysis method.

2.1. Theory of temporal and spectral CSD

CSD analysis was first proposed in the 1950s (Howland et al., 1955; Pitts, 1952). Since then it has been formalized extensively in subsequent studies (Bedard and Destexhe, 2011; Freeman and Nicholson, 1975; Mitzdorf, 1985; Nicholson and Llinas, 1975; Schroeder et al., 1998). A standard CSD analysis of brain activity rests on a series of assumptions: ohmic conductive medium, constant extracellular conductivity, homogeneous in-plane neuronal activity, and equidistant laminar electrode contacts. From the continuity condition of current flow, the CSD denoted by $I_t(x, y, z)$ in a small volume element is the divergence of current flow density (J) from the surface of that element. Furthermore, it is related to the negative of Laplacian of the LFP $\Psi_t(x, y, z)$ (Mitzdorf, 1985; Nicholson and Freeman, 1975) under the assumption of a purely ohmic conductive medium:

$$I_t = -\nabla.(\sigma\nabla\Psi_t), \tag{1}$$

The CSD can be transformed into the frequency (f) domain from the time (t) domain using direct Fourier transform (Bedard and Destexhe, 2011). In the frequency domain, Eq. (1) can be rewritten as:

$$I_\omega = -\nabla.(\sigma\nabla\Psi_\omega), \tag{2}$$

where $\Psi_\omega(z) = \int_{-\infty}^{+\infty} \Psi_t(z)\exp(-i\omega t)\,\mathrm{d}t$ and $\omega = 2\pi f$. If the outward currents dominate in a volume element, a current source results ($I > 0$) from cations flowing out to the extracellular space. If the inward currents dominate, a current sink results from cations flowing into the intracellular space ($I < 0$). σ is the symmetric conductivity tensor which can be made diagonal through a linear transformation (Freeman and Nicholson, 1975).

2.1.1. Laminar (one-dimensional) local field potentials (LFPs)

The laminar LFPs are recorded under the assumptions that: (i) the fiber bundles of dendrites are elongated along the z-axis, (ii) conductivity is homogeneous, and (iii) dominant current flows are along the elongated structures only, then Eqs. (1) and (2) reduce to:

$$I_t = -\sigma_z \left[\partial^2 \Psi_t / \partial z^2\right], \qquad I_\omega = -\sigma_z \left[\partial^2 \Psi_\omega / \partial z^2\right], \tag{3}$$

where z-axis is perpendicular to the cortical layers and $\sigma_z = \sigma$ is a constant.

Experimentally, the spatiotemporal LFP is generally recorded using a linear array electrode with discrete equidistant locations from several layers of the cortex. The second spatial derivative is then estimated by the following 3-points, finite-difference formula (Freeman and Nicholson, 1975; Mitzdorf, 1985):

$$\frac{\partial^2 \Psi_\omega(z)}{\partial z^2} \approx \frac{\Psi_\omega(z+\Delta z) - 2\Psi_\omega(z) + \Psi_\omega(z-\Delta z)}{(\Delta z)^2}, \tag{4}$$

where Δz is a distance between adjacent recording sites. If N is the number of electrodes or channels, the negative value of Eq. (4) renders the CSD profiles at the $N-2$ interior electrode positions. The profiles at the first and last electrode locations can be estimated by the extrapolation technique of LFPs, but are usually left undefined (Chen et al., 2008).

Finally, the CSD profiles at a particular frequency are given by the negative of the second spatial derivative of Ψ_ω:

$$I_\omega \propto -\left[\partial^2 \Psi_\omega / \partial z^2\right], \tag{5}$$

where the term on right side is approximated by Eq. (4), and Ψ_ω the spectral factor computed from SF as discussed in Section 2.2.

In the time-domain, a neural signal is represented by its magnitude at each time point. In the frequency-domain, $\Psi_\omega(z) = A + iB$, where A and B are the real and the imaginary parts respectively. The neural signal is then represented by its magnitude and phase expressed as $\sqrt{A^2+B^2}$ and $\tan^{-1}(B/A)$ respectively at each frequency. In a similar fashion, the CSD is expressed as: $\Psi_\omega = C + iD$, and $|I_\omega| = \sqrt{C^2+D^2}$. The CSD power, which is a square of magnitude by definition, is $|I_\omega|^2$. Furthermore, the phase information is within I_ω, but when we calculate $|I_\omega|^2$, it has not been considered. The phase, represented by θ, is calculated using the general definition, $\theta = \tan^{-1}(D/C)$. The SF-CSD profiles considered throughout the text are $|I_\omega|^2$ multiplied by cosine of θ at each frequency.

2.1.1.1. Simulated LFPs data. The spontaneous spatiotemporal signals, similar to those recorded in electrophysiological experiments, can be generated from the mathematical models for spatial and temporal dynamics (Chen et al., 2008). The SF-CSD algorithm is then used to compute the SF-CSD patterns. The validity of our SF-CSD method is assessed by comparing the SF-CSD patterns with the known input mathematical functions. This kind of direct cross-validation is not possible in the analysis of real electrophysiological data where the answer is not known a priori.

Experimentally, the data to be analyzed comes from a cortical column. In this study, we have laminar LFP recordings from the inferior-temporal cortex of a monkey. Here a cortical column is sampled at equal distances. In simulation, the spatiotemporal signal $\Psi_t(z)$ is obtained by multiplying the space- and time-dependent functions (Chen et al., 2008):

$$\Psi_t(z) = \Phi(z)\psi(t), \tag{6}$$

The spatial part $\Phi(z) = C_1 z + C_2 - A_z \operatorname{Cos}(2\pi f_z z + \theta_z)/(2\pi f_z)^2$ is obtained by integrating the second spatial derivative, represented by one sinusoidal profile (a source-sink pair) and also by two independent sinusoidal profiles (two source-sink pairs), $[\partial^2\Phi(z)/\partial z^2] = A_z \operatorname{Cos}(2\pi f_z z + \theta_z)$. Here, C_1 and C_2 are constants. A_z, f_z, θ_z $(=-\pi/2)$ are amplitude, frequency and phase for spatial dynamics respectively. The temporal dynamics can be either a sinusoidal function $A_t \operatorname{Sin}(2\pi f_t t + \theta_t)$ or the function in a second order autoregressive (AR2) process expressed as: $\psi(t) = a\psi(t-1) + \beta\psi(t-2) + \xi(t)$. Here, A_t, f_t, θ_t are amplitude, frequency and phase for temporal dynamics respectively and $\alpha = 0.55$ and $\beta = -0.70$ are constants and ξ is a white Gaussian noise. In the present case, AR(2) is chosen for the temporal dynamics. The model is simulated with the following parameter values: number of time points in the signal = 200, number of trials = 500 and sampling rate (f_s) = 200 Hz. In parametric (P) spectral estimation (as shown in Fig. 2), Morf's autoregressive (AR) model of order 2 (Dhamala et al., 2008b; Morf et al., 1978) has been used. For the nonparametric (NP) approach, the value of 'time half bandwidth product' we used is 3 in multitaper spectral estimation (Dhamala et al., 2008a).

2.1.1.2. Experimental LFPs data. The SF-CSD is applied to laminar LFPs recorded from a monkey performing an intermodal selective attention task (either ignore or attend to the visual stimuli). The data considered here are from a previously published study (Mehta et al., 2000a,b) in which a macaque monkey was trained to discriminate stimuli in both the auditory and visual domains. In the first condition, a mixed stream of auditory and visual stimuli was presented. A standard and odd ball stimulus occurred 86% and 14% of the time respectively in each sensory modality. The monkey was instructed to respond to the oddball stimulus in the attended modality only. In the second condition, the monkey performed the oddball detection task in the auditory domain without visual stimulus. The analysis of activity in visual cortices during auditory discrimination represents the spontaneous ongoing neural activity keeping the monkey verifiably alert in the absence of visual stimulus. The LFPs were sampled with a linear array of electrodes consisting of 14 contacts with 150 μm inter-contact spacing and spanning all six layers in the inferior-temporal cortex. The data consists of the following parameter values: number of time points in the LFPs = 401, number of trials = 418 and sampling rate = 2000 Hz.

2.2. Spectral factorization (SF)

The SF was first proposed by Wiener (1949) for a single time series and was further formalized for multiple time series in subsequent studies (Wiener and Masani, 1957; Youla, 1961). Since then, it has been widely applied in the fields of digital signal processing, control theory, communications, geophysics and neuroscience (Dhamala et al., 2008a).

The spectral function $S(\omega)$ is defined in the interval $[-\pi, \pi]$, and for all practical purposes, it satisfies the following properties (Wilson, 1972, 1978): (i) $S(\omega)$ is non-negative $S(-\omega) = S(\omega)$, and (ii) $S(\omega)$ is integrable and has a Fourier series expansion: $S(\omega) = \sum_{k=-\infty}^{\infty} \beta_k \exp(i\omega k)$, where $\beta_k = \frac{1}{2\pi}\int_{-\pi}^{+\pi} S(\omega) \exp(-i\omega k) d\omega$ and $\omega = 2\pi f$. The plus operator is then expressed as, $[S(\omega)]^+ = (\beta_0/2) + \sum_{k=1}^{\infty} \beta_k \exp(i\omega k)$ i.e., 'the half of zero-component' plus 'all other components of positive side'. The spectral function $S(\omega)$, satisfying $\int_{-\pi}^{+\pi} \log S(\omega) d\omega > -\infty$, can be factorized into a set of unique minimum-phase functions:

$$S = \Psi_\omega \Psi_\omega *, \tag{7}$$

where * denotes complex conjugate and the term minimum-phase means the spectral factor (Ψ_ω), defined on the unit-circle $C = \{|z| = 1\}$, has no zero lying outside the circle (Orchard and Willson, 2003; Wilson, 1972). Here, Ψ_ω is the averaged spectral factor (see Table 1: step-by-step algorithm) similar to the averaged LFP in time domain, and contains the phase information, a crucial information needed to compute SF-CSD. Furthermore, (a) Ψ_ω has a Fourier series expansion in nonnegative powers of $\exp(i\omega)$: $\psi_\omega = \sum_{k=0}^{\infty} A_k \exp(i\omega k)$, and (b) it can be holomorphically extended to the inner disk $\{|z| < 1\}$ as $\Psi_\omega = \sum_{k=0}^{\infty} A_k z^k$. Using the logarithmic law,

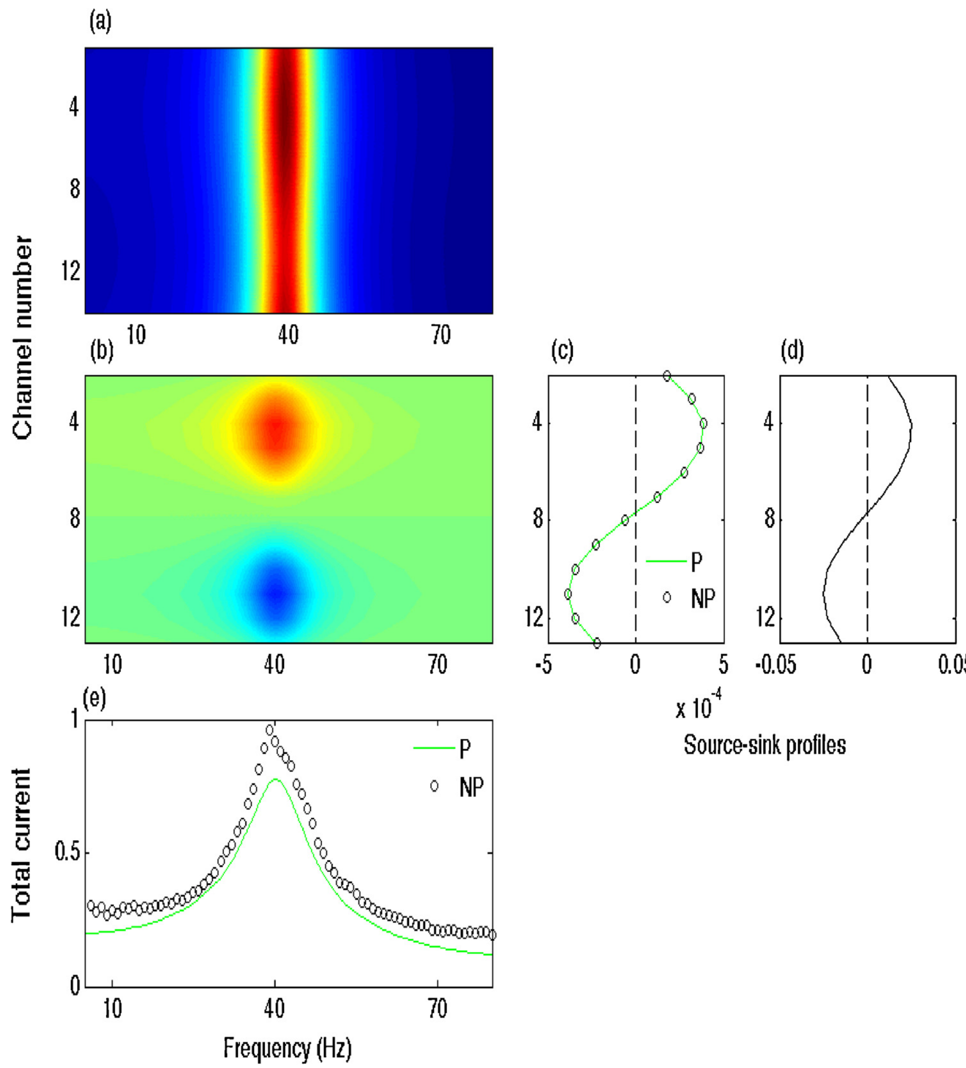

Fig. 2. The simulated single source-sink pair at 40 Hz. (a) Color-coded average spectral power profiles as a function of depth 2-13 (channel number) and frequency 5-80 Hz, (b) the SF-CSD profiles as a function of depth 2–13 and frequency 5–80 Hz, (c) a source-sink pair in the SF-CSD using both the parametric (P) and nonparametric (NP) approaches, (d) the source-sink profiles of the initial mathematical function. Panel (e) is the total current (the SF-CSD averaged over channels) for both the P and NP approaches. (For interpretation of the references to color in this figure legend, the reader is referred to the web version of the article.)

one can write $\log S(\omega) = \log \Psi_\omega + \log \Psi^*_\omega$. From the condition, one can expand as: $\log S(\omega) = \sum_{k=-\infty}^{\infty} \alpha_k \exp(i\omega k)$. Also, from the properties (a, b) of Ψ_ω, one can expand as: $\log \Psi_\omega = \sum_{k=0}^{\infty} \beta_k \exp(i\omega k)$. Thus, one can obtain the following expression (Wilson, 1972):

$$\Psi_\omega = \exp\,[\log S(\omega)]^+, \tag{8}$$

where $S(\omega)$ is known before SF (see Table 1: step-by-step algorithm) and $[.]^+$ is computed from the sum of 'the half of zero-component' plus 'all other components of positive side' of 'log $S(\omega)'$' (Wilson, 1972).

The spectral factor (Ψ_ω) can then be used to numerically estimate SF-CSD profiles in Eq. (4). The step-by-step algorithm for the SF-CSD is presented in Table 1. Electrophysiological data, including local field potentials (LFPs), are noisy. By using a spectral factor of ensemble averaged spectra in the CSD calculation as in Eq. (8), we can minimize the effect of noise amplification in CSD estimates. When the spectral power undergoes spectral factorization, as shown above, a spectral factor defined on the unit circle has no zero lying outside that unit-circle and hence the factor comes out to be minimum-phase (Orchard and Willson, 2003; Wilson, 1972). This is consistent with the idea that the initial overall average phase is minimum (close to zero) for an ensemble of non-phase locked trials within a channel.

Table 1
The step-by-step SF-CSD algorithm: (1) extract epochs of ongoing activity ('n' represents the number of trials), (2) take Fourier transform of ongoing brain activity, (3) compute the average spectral power from an ensemble of trials, (4) factorize (by using spectral factorization) the averaged spectral power, (5) compute CSD, and (6) compute CSD power and phase.

1. Extract epochs of ongoing brain activity: $\Gamma_t^n(z)$
2. Take Fourier transform of $\Gamma_t^n(z)$: $\Gamma_\omega^n(z)$
3. Compute average spectral power: $S = \frac{1}{N}\sum_{n=1}^{N} \Gamma_\omega^n(z)\Gamma_\omega^n(z)^*$
4. Factorize S: $S = \Psi_\omega(z)\Psi_\omega(z)^*$
5. Compute CSD: $I_\omega\, \alpha - \partial^2\Psi_\omega/\partial z^2$
6. Compute CSD power ($|I_\omega|^2$) and phase (θ) from $I_\omega = C + iD$: $|I_\omega|^2 = (C^2 + D^2)$ and $\theta = \tan^{-1}(D/C)$

3. Results

3.1. Simulated LFPs data

The models (Section 2.1.1.1) are simulated and the data are assumed to be acquired from a linear array electrode with 14

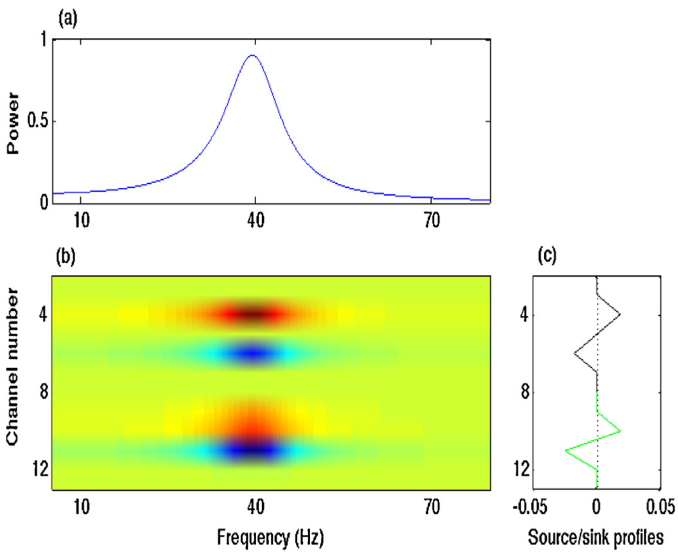

Fig. 3. The simulated multiple independent source-sink pairs at 40 Hz. (a) Normalized average spectral power profiles as a function of frequency 5-80 Hz, (b) the SF-CSD profiles as a function of depth 2–13 and frequency 5–80 Hz, and (c) the source-sink profiles of the initial mathematical function.

equally spaced contacts. The results of simulated LFP that include the SF-CSDs for a source-sink pair and two independent source-sink pairs respectively are presented below.

3.1.1. SF-CSD for a source-sink pair

Fig. 2 shows the results for the averaged power spectra (S) and the SF-CSD profiles for a source-sink pair at 40 Hz temporal dynamics.

In Fig. 2, panel (a) shows the averaged spectral power (called power spectra) over trials of ongoing oscillation as a function of electrode sites and frequency (5–80 Hz), where temporal dynamics at 40 Hz are dominant. The SF-CSD profiles consisting of a source-sink (red and blue color-coded) pair are clearly seen at around electrode sites 4 and 11. Both parametric (P) and nonparametric (NP) approaches (Dhamala et al., 2008a,b) are used. The SF-CSD profiles averaged over frequency in both P and NP approaches are shown in panel (c), illustrating a good agreement between these approaches. A source-sink pair of known initial mathematical function is presented in panel (d). Comparing panels (c) and (d), we can see that the SF-CSD algorithm uncovers a hidden source-sink pair oscillating at a frequency of 40 Hz. Furthermore, panel (e) shows the normalized total current (the SF-CSD averaged over channels) for both P and NP approaches. This technique again correctly reveals the underlying spatiotemporal source-sink pair accentuating the importance of the SF-CSD analysis to precisely localize the oscillating generators.

3.1.2. SF-CSD for two independent source-sink pairs

The study of the SF-CSD is extended for two independent source-sink pairs.

Fig. 3 shows the results for the averaged spectral power and the SF-CSD profiles. Panel (a) shows the normalized average power spectra over trials of ongoing oscillation versus frequency (5–80 Hz), where the oscillation at 40 Hz is dominant. The SF-CSD profiles, shown in panel (b), are seen at electrode sites 4, 6, 10, and 11. To ensure source-sink pairs of panel (b), independent source-sink pairs of known initial mathematical function are presented in panel (c). For clarity, we have colored the independent oscillators in black and green. These two panels support that the SF-CSD algorithm uncovers the hidden independent source-sink pairs oscillating at a frequency of 40 Hz.

3.2. Experimental LFPs data

The SF-CSD method is then applied to the LFP recordings, taken from the inferior-temporal cortex of a monkey performing intermodal selective attention tasks, consisting of 14 equally spaced contacts in a linear array electrode. The averaged spectral power and the SF-CSD profiles are displayed in Fig. 4.

The first row of plots (a, b) is for the visual ignore (I) and the second row (c, d) is for the visual attend (A), while plot (e) is the comparison between two. Panels (a) and (c) show the averaged spectral power at 10 Hz (alpha oscillation) distributed at different electrode sites for visual ignore and attend conditions respectively. The SF-CSD profiles are shown in panels (b) and (d). Panels (b) and (d) show that the dominant SF-CSD patterns are in the supragranular layer (around contacts 3–7) and absent from the granular layer (layer 4, around contacts 8–10) and very weak patterns in infra-granular (around contacts 10–11). Furthermore, panel (e) shows the total current (i.e., the SF-CSD averaged over channels) peaked at 10 Hz during both visual attend and visual ignore conditions.

4. Discussion

In this work, we introduced the SF-CSD analysis for ongoing neural oscillations. Here, we presented the theory, verified the method using simulations, and demonstrated the utility of the method in the physiological recordings of LFP. This method provides the results in the form of CSD spectra (the transmembrane currents in terms of sources and sinks) as a function of frequency and space. The spectral factor as obtained from SF is used to localize the transmembrane current. In this method, the SF-CSD profile is computed in this sequence: (1) extract epochs of ongoing activity, (2) take Fourier transform of ongoing brain activity, (3) compute the average spectral power from an ensemble of trials, (4) factorize (by using spectral factorization) the averaged spectral power, (5) compute CSD, (6) compute CSD power and phase. The SF-CSD profiles are then expressed as CSD power times cosine of phase. This method is applicable not only to ongoing oscillations, but also to neural activity (evoked and/or induced) related to external stimuli since the wavelet spectral method can be used to estimate power spectra from non-stationary signals like the evoked or induced brain activity (see Appendix for the SF-CSD of induced oscillation). Here, we applied our method to previously published data (Mehta et al., 2000a,b) consisting of LFPs from 6-brain layers of the inferior-temporal cortex of a monkey and obtained excellent agreement with the published results.

Similar to the traditional time-domain CSD method, the SF-CSD method renders the activity free from any non-local, first order spatial effects such as volume conduction. Here, the theoretical framework is presented for electrical recordings of ongoing oscillation in one dimension (i.e., LFPs) based on the assumptions: elongated fiber bundles of dendrites along the z-axis, homogeneous conductivity, dominant current flow along elongation, and equidistant electrode contacts. We illustrated applicability of the SF-CSD algorithm using the LFP simulated data. We checked the SF-CSD algorithm using both parametric (P) and nonparametric (NP) approaches. It worked reliably well for both single source-sink pair and multiple independent neural source-sink pairs. As the source and sink profiles are identified by the phase information, it also works for multiple dependent source-sink pairs. The SF-CSD algorithm is then applied to the laminar LFPs recorded from a monkey performing an intermodal selective attention task

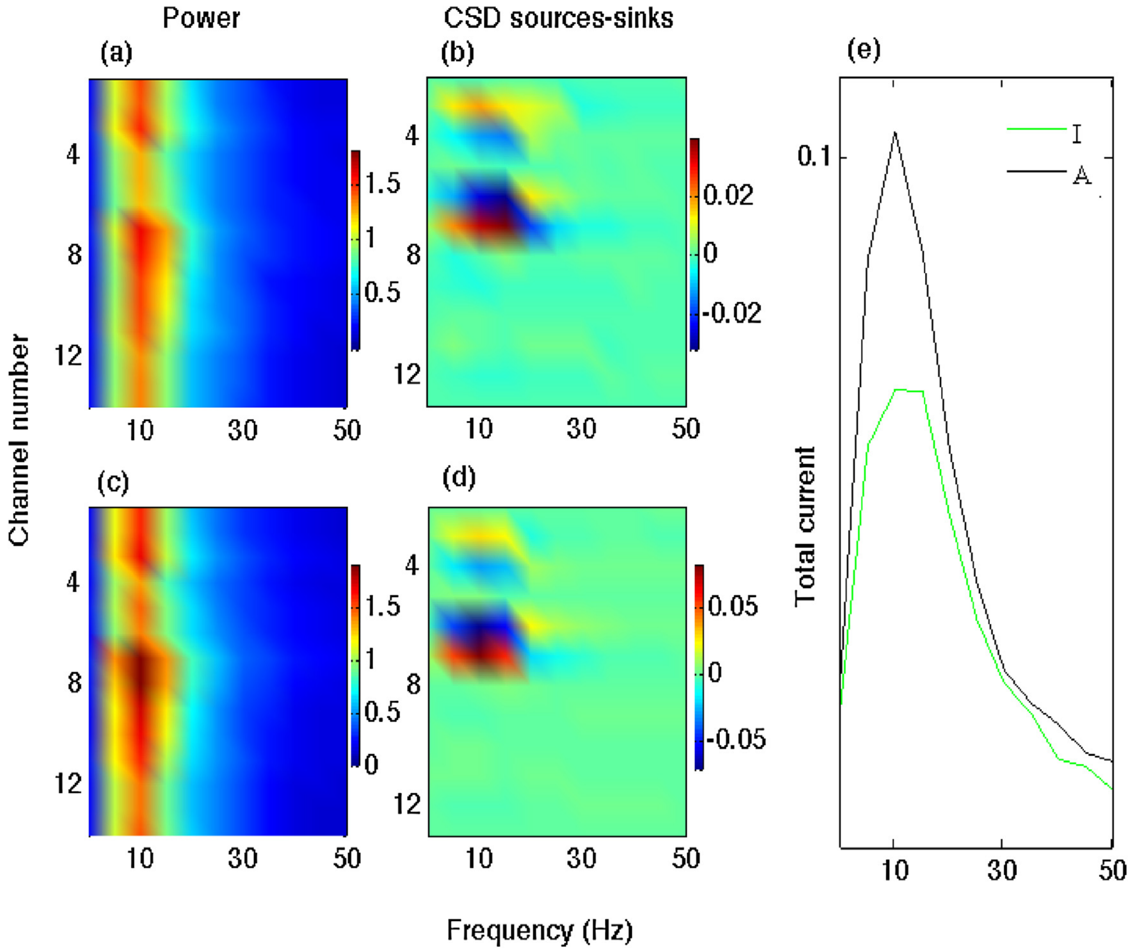

Fig. 4. The SF-CSD analyses of the LFP recordings from the monkey's inferio-temporal cortex for visual ignore (I) [(a), (b)] and visual attend (A) [(c), (d)]. Panels (a) and (c) represent the average spectral power as a function of electrode locations (channel number) and frequency 0-50 Hz. Panels (b) and (d) are the SF-CSD source-sink profiles as a function of electrode locations and frequency 0-50 Hz. Panel (e) shows the total current (the SF-CSD averaged over channels) compared between I and A conditions.

(either visual ignore or attend). The data considered here is from a previously published study (Dhamala et al., 2006; Mehta et al., 2000a,b). The results showed dominant SF-CSD patterns in the supra-granular layers (around contacts 3–7), absent from the granular layer (around contacts 8–10) and very weak patterns in infra-granular layer (around contacts 10–11). These patterns are consistent with the idea that the top-down brain network signals only engage supra- or infra-granular layers (Felleman and Van Essen, 1991). The study can be further extended to the case of inhomogeneous medium by taking the space-dependent conductivity values (Nakagawa and Matsumoto, 2000).

In the time-domain, a neural signal is represented by its magnitude at each time point and the corresponding waveform is detected by peak activity (Csicsvari et al., 2003). However, ongoing oscillation is problematic in the time-domain because ensemble averaging as shown in Fig. 1 muffles activity. The frequency-domain, where an ongoing neural signal is represented by its amplitude and phase at each frequency, preserves phase information in the spectral factor and ultimately in the SF-CSD profiles too. The CSD profiles, which are free from non-local, first order spatial effects like volume conduction, can be further used to study the interactions between various brain regions or layers by implementing the idea of coherence (Csicsvari et al., 2003). As we have computed the SF-CSD profiles for each frequency from the spectral factor, a common question is whether the spectral power can uncover the same spatial patterns or not. A source localization technique such as the CSD cannot directly be implemented to the spectral power because of the following reasons: first, the spectral power comprises squared LFP and therefore the polarity information contributed by the phase angle is lost, and second, the spectral power is reference-dependent (Michel et al., 2004). In contrast, the SF-CSD pattern derived from the spectral factor eliminates those issues. The proposed SF-CSD method opens up an alternative way to compute CSD patterns of ongoing neural oscillations without considering the reference channel as previously used PRAT-based CSD (Chen et al., 2008; Dhamala et al., 2006) needs the reference channel. However, there is always some level of error in the CSD (even in the SF-CSD) profiles such as the approximation of second spatial derivative of the LFP [i.e., error $1/\Delta z^2$ in Eq. (4)] (Freeman and Nicholson, 1975) and some unavoidable inherent noise in the LFP recordings.

For decades, CSD analysis has been a very useful tool to show the spatiotemporal patterns of synaptic events in electrically evoked responses (Nakagawa and Matsumoto, 2000). In recent years however, there is a growing interest in the study of ongoing neural activity and its role in various brain functions (Arieli et al., 1996; Chen et al., 2008; Csicsvari et al., 2003; Dehaene et al., 2003; Lakatos et al., 2005). The study of hierarchical interactions of cortical layers from different brain areas (Felleman and Van Essen, 1991; Raizada and Grossberg, 2003) is on the forefront of neuroscience research. The technology for multi-electrode neurophysiological recordings is rapidly evolving with better and finer electrodes (Buzsaki, 2004;

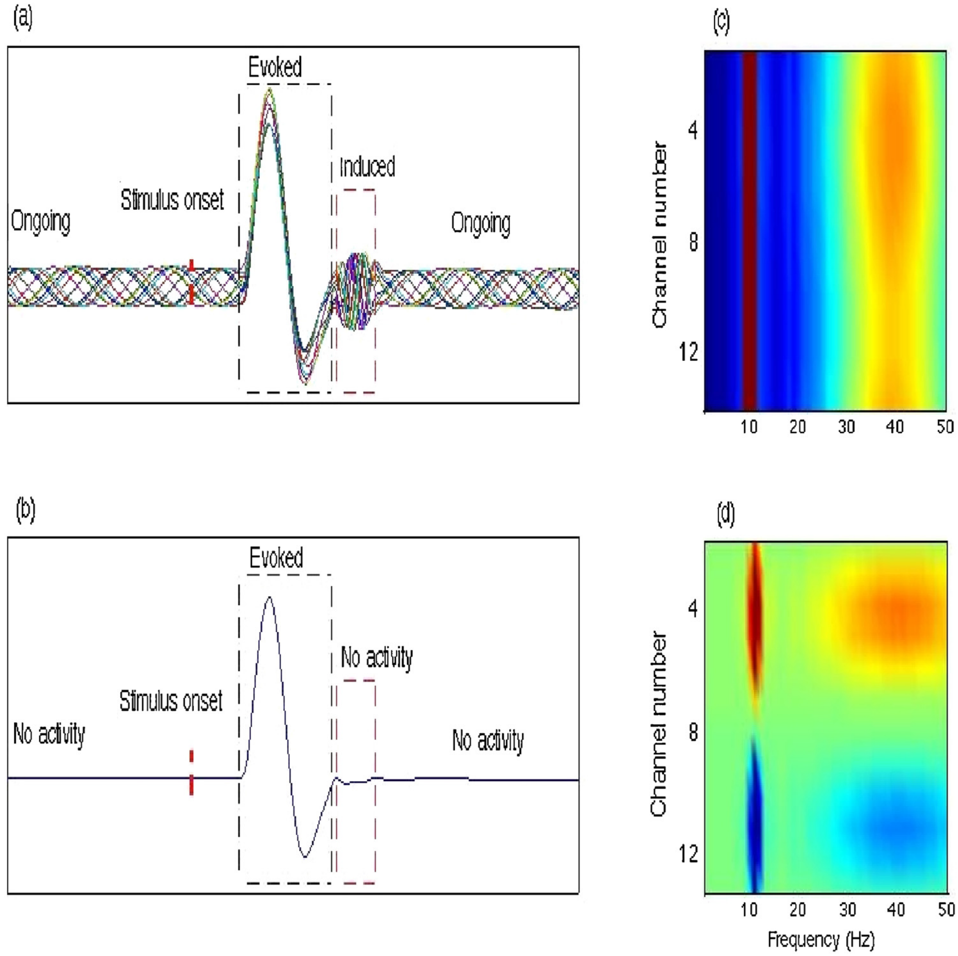

Fig. A1. Panel (a) shows superimposed responses with ongoing, evoked, and induced activities, Panel (b) shows the average waveform from ensemble averaging: ongoing and induced activities are completely suppressed and only stimulus phase-locked evoked activity is retained, Panel (c) shows the spectral power of evoked (10 Hz) and induced (40 Hz) activities, and Panel (d) shows the SF-CSD profiles obtained for evoked and induced activities. These results suggest that ongoing and induced activities (a) can be averaged out (b) in a stimulus-triggered average, but can be observed using the SF-CSD analysis (d) removing common spatial effects as seen in the averaged spectral power distributions over channels (c). In (d), we recover the source-sink patterns at channels 4 and 11 for induced activity oscillating at 40 Hz. The spectral power and the SF-CSD shown for evoked activity oscillating at 10 Hz are from averaged time-series.

Lakatos et al., 2005; Mehta et al., 2000a,b). In light of these interests and evolving electrode technology, we believe the proposed SF-CSD method to be a useful tool in advancing the systematic analysis of ongoing electrophysiological oscillations for the neuroimaging community.

Acknowledgements

We would like to thank Charles E. Schroeder and Mingzhou Ding for providing us the previously published electrophysiological data from a monkey (Dhamala et al., 2006; Mehta et al., 2000a,b). We would also like to thank Kristen Quinn for reading the initial manuscript and providing us corrections. The author MD would like to acknowledge the NSF Grant support (CAREER Award BCS 0955037).

Appendix.

The SF-CSD algorithm can also be used to examine oscillations from trials containing induced activity which is time-locked but phase-unlocked from trial to trial.

See Fig. A1.

References

Arieli A, Sterkin A, Grinvald A, Aertsen A. Dynamics of ongoing activity: explanation of the large variability in evoked cortical responses. Science 1996;273:1868–78.

Bazhenov M, Lonjers P, Skorheim S, Bedard C, Destexhe A. Non-homogeneous extracellular resistivity affects the current source density profiles of up-down state oscillations. Philos Trans R Soc A 2011;369:3802–19.

Bedard C, Destexhe A. Generalized theory for current source density analysis in brain tissue. Phys Rev E 2011;84:041909.

Buzsaki G. Large-scale recording of neuronal ensembles. Nat Neurosci 2004;7:446–51.

Buzsaki G. Rhythms of the brain. NY, USA: Oxford University Press, Inc; 2006.

Buzsaki G, Anastassiou CA, Koch C. The origin of extracellular fields and currents – EEG, ECoG, LFP and spikes. Nat Rev 2012;13:407–20.

Buzsaki G, Draguhn A. Neuronal oscillations in cortical networks. Science 2004;304:1926–9.

Chen Y, Dhamala M, Bollimunta A, Schroeder CE, Ding M. Current source density analysis of ongoing neural activity. Electrophysiological Recording Methods. Totowa, NJ, USA: Human Press; 2008.

Csicsvari J, Jamieson B, Wise K, Buzsaki G. Mechanics of gamma oscillations in the hippocampus of the behaving rat. Neuron 2003;37:311–22.

Dehaene S, Sergent C, Changeux JP. A neuronal network model linking subjective reports and objective physiological data during conscious perception. Proc Natl Acad Sci USA 2003;100:8520–5.

Dhamala M, Rangarajan G, Ding M. Analyzing information flow in brain networks with nonparametric Granger causality. NeuroImage 2008a;41:354–62.

Dhamala M, Rangarajan G, Ding M. Estimating Granger causality from Fourier and wavelet transforms of time series data. Phys Rev Lett 2008b;100(018701):018701–4.

Dhamala M, Schroeder CE, Ding M. Atttentional modulation of cortical ongoing neural oscillations. Soc Neurosci Abstr 2006, Prog. No. 160.11.

Felleman DJ, Van Essen DC. Distributed hierarchical processing in the primate cerebral cortex. Cereb Cortex 1991;1:1–47.
Fiser J, Chiu C, Weliky M. Small modulation of ongoing cortical dynamics by sensory input during natural vision. Nature 2004;431:573–8.
Freeman JA, Nicholson C. Experimental optimization of current source density technique for anuran cerebellum. J Neurophysiol 1975;38:369–82.
Howland B, Lettvin JY, McCulloch WS, Pitts W, Wall PD. Reflex inhibition by dorsal root interaction. J Neurophysiol 1955;18:1–17.
Kajikawa Y, Schroeder CE. How local is the local field potential? Neuron 2011;72:847–58.
Kenet T, Bibitchkov D, Tsodyks M, Grinvald A, Arieli A. Spontaneously emerging cortical representations of visual attributes. Nature 2003;425:954–6.
Lakatos P, Shah AS, Knuth KH, Ulbert I, Karmos G, Schroeder CE. An oscillatory hierarchy controlling neuronal excitability and stimulus processing in the auditory cortex. J Neurophysiol 2005;94:1904–11.
Mehta AD, Ulbert I, Schroeder CE. Intermodal selective attention in monkeys. I: distribution and timing of effects across visual areas. Cereb Cortex 2000a;10:343–58.
Mehta AD, Ulbert I, Schroeder CE. Intermodal selective attention in monkeys. I: physiological mechanisms of modulation. Cereb Cortex 2000b;10:359–70.
Michel CM, Murray MM, Lantz G, Gonzalez S, Spinelli L, Grave de Peralta R. EEG source imaging. Clin Neurophysiol 2004;115:2195–222.
Mitzdorf U. Current source density method and application in cat cerebral cortex: investigation of evoked potentials and EEG phenomenon. Physiol Rev 1985;65:37–100.
Morf M, Vieira A, Lee DTL, Kailath T. Recursive multichannel maximum entropy spectral estimation. IEEE Transact Geosci Electron 1978;GE-16:85–94.
Nakagawa H, Matsumoto N. Current source density analysis of ON/OFF channels in the frog optic tectum. Prog Neurobiol 2000;61:1–44.
Nicholson C, Freeman JA. Theory of current source-density analysis and determination of conductivity tensor for anuran cerebellum. J Neurophysiol 1975;38:356–68.
Nicholson C, Llinas R. Real time current source-density analysis using electrode array in cat cerebellum. Brain Res 1975;100:418–24.
Orchard HJ, Willson AN. On the computation of a minimum-phase spectral factor. IEEE Trans Circuits Syst 2003;50:365–75.
Pitts W. Investigation on synaptic transmission. In: Von Foerster, editor. Cybernetics, trans. 9th conf. NY, USA: Josiah Macy Foundation; 1952. p. 159–66.
Raizada RDS, Grossberg S. Towards a theory of the laminar architecture of cerebral cortex: computational clues from the visual system. Cerebral Cortex 2003;13:1000–113.
Schroeder CE, Mehta AD, Givre SJ. A spatiotemporal profile of visual system activation revealed by current source density analysis in the awake macaque. Cereb Cortex 1998;8:575–92.
Tsodyks M, Kenet T, Grinvald A, Arieli A. Linking spontaneous activity of single cortical neurons and the underlying functional architecture. Science 1999;286:1943–6.
Wiener N. Extrapolation, interpolation and smoothing of stationary time series with engineering applications. New York: Wiley; 1949.
Wiener N, Masani P. The prediction theory of multivariate stochastic processes. I Acta Math 1957;98:111–50 (II. Acta Math 99, 93–137).
Wilson GT. The factorization of matricial spectral densities. SIAM J Appl Math 1972;23:420–6.
Wilson GT. A convergence theorem for spectral factorization. J Multivar Anal 1978;8:222–32.
Youla DC. On the factorization of rational matrices. IRE Trans Inf Theory 1961;7:172–89.